npj | climate and atmospheric science

Brief communication

Published in partnership with CECCR at King Abdulaziz University

https://doi.org/10.1038/s41612-025-01121-w

Unravelling drivers of the future Mediterranean precipitation paradox during cyclones

Marco Chericoni[1,2,3] ✉, Giorgia Fosser[1], Emmanouil Flaounas[4], Marco Gaetani[1] & Alessandro Anav[2,3]

Both global climate models and a high-resolution atmosphere-ocean coupled regional climate model project a drying trend across the Mediterranean region, alongside an increase in cyclone-related precipitation. However, only the high-resolution model captures the physical mechanisms driving these changes across three emission scenarios, namely, enhanced moisture transport processes fuelling cyclone activity. These results highlight the added value of fine-scale modelling for understanding future Mediterranean hydroclimatic extremes.

Recent floods in southern Europe, primarily driven by extratropical cyclones and intensified by climate change, have had severe socioeconomic consequences. Notable episodes include the floods in central Italy in 2023[1] and in Valencia in 2024[2], both resulted in large economic losses, societal disruption, and fatalities. Additionally, the Mediterranean basin is increasingly recognised as a climate change hotspot[3,4]. For these reasons, understanding the impact of climate change on the interplay between cyclones and precipitation is more critical than ever.

Mediterranean cyclogenesis is driven by upper-tropospheric systems, caused by Rossby wave breaking over the Atlantic[5], especially during the extended cold season (October–March, ONDJFM)[6]. Cyclone development relies on both baroclinic forcing and deep convection near its centre, which enhances potential vorticity and intensification[7]. Maximum intensity typically occurs over maritime areas like the Gulf of Genoa, Adriatic, Ionian and Aegean Seas[5]. Global warming increases atmospheric moisture and surface potential energy available for convection, fostering moisture uplift and thus the precipitable water during cyclones[8]. However, changes in baroclinicity can either amplify or inhibit these processes, highlighting the complex interplay of factors influencing Mediterranean precipitation response to climate change.

CMIP5-based studies[6,9] highlight a climate paradox for future Mediterranean precipitation: while total precipitation is expected to decline due to reduced cyclonic activity, cyclone-related precipitation is projected to increase in the north-central Mediterranean but decrease in the southeast. However, models show large disagreement, and the underlying mechanisms are not yet fully understood.

This study aims to bridge these knowledge gaps by investigating how changes in moisture transport processes locally impact cyclone-related precipitation[10]. This is essential for improving confidence in climate projections and attributing changes to climate change[11]. Both global (CMIP6, Coupled Model Intercomparison Project Phase 6) and regional (ENEA-REG[12]) climate projections (Table 1) are used to evaluate changes in Mediterranean cyclones characteristics and associated precipitation under three Shared Socioeconomic Pathways[13] (SSP5-8.5, SSP2-4.5, and SSP1-2.6). ENEA-REG is the only available high-resolution atmosphere-ocean coupled regional climate model (AORCM) in the Med-CORDEX initiative[14] covering all scenarios. Mediterranean cyclones are tracked in all simulations within the Med-CORDEX domain (Fig. S1), for the period 1982–2100. The analysis focuses on the most intense cyclones, i.e., with a minimum SLP below 1000 hPa along the life cycle, during the extended cold season, when their influence on precipitation and wind speed is stronger. In supplementary information, the regional and global models are compared to an ensemble of high-resolution CMIP6 and against ERA5 reanalysis data, to assess their ability in reproducing the seasonal cycle (Fig. S8) and spatial distribution (Fig. S9) of intense Mediterranean cyclones during the historical period (1985–2014).

Both ENEA-REG and the ensemble of CMIP6 simulate a significant decrease in the number of intense Mediterranean cyclones (34–39% under SSP5-8.5; Fig. 1a) and in seasonal precipitation (12–14% under SSP5-8.5; Fig. 1b) with increasing greenhouse gas (GHG) emissions across the three SSP scenarios. In clear contrast, extreme (99th percentile) precipitation associated with these cyclones (Fig. 1c) is projected to increase by up to ~19% by the end of the century under the high-emission scenario (SSP5-8.5). This intensification aligns with radiative forcing trends under the various scenarios[13] (inset Fig. 1a), as increased energy in the atmosphere fuels these cyclonic events. Notably, ENEA-REG simulates more intense cyclones and stronger extreme precipitation than the CMIP6 ensemble, benefiting from its finer resolution[15].

Despite the large spread in future projections, reflected by the standard deviation among CMIP6 models (shaded areas in Fig. 1), our analysis

[1]University School for Advanced Studies IUSS, Pavia, Italy. [2]Italian National Agency for New Technologies, Energy and the Environment (ENEA), Rome, Italy. [3]ICSC Italian Research Center on High-Performance Computing, Big Data and Quantum Computing, Bologna, Italy. [4]Institute of Oceanography, Hellenic Centre for Marine Research, Athens, Greece. ✉e-mail: marco.chericoni@iusspavia.it

Table 1 | List of analysed regional and global climate models

Type of model	Model name	Institution	Atmospheric horizontal resolution
Regional climate model	ENEA-REG[12]	ENEA, Italy	12 km
CMIP6	BCC-CSM2-MR[28]	BCC, China	100 km
CMIP6	CMCC-ESM2[29]	CMCC, Italy	100 km
CMIP6	EC-Earth3[30]	European Consortium, Europe	80 km
CMIP6	MPI-ESM1.2-HR[31]	MPI, Germany	80 km
CMIP6	MRI-ESM-2.0[32]	MRI, Japan	100 km
CMIP6	NorESM2-MM[33]	NCC, Norway	100 km
CMIP6-HR	BCC-CSM2-HR[34]	BCC, China	40 km
CMIP6-HR	CMCC-CM2-VHR4[35]	CMCC, Italy	25 km
CMIP6-HR	CNRM-CM6.1-HR[36]	CNRM, France	50 km
CMIP6-HR	EC-Earth3P-HR[37]	European Consortium, Europe	40 km
CMIP6-HR	ECMWF-IFS-HR[38]	ECMWF, Europe	30 km
CMIP6-HR	GFDL-CM4C192[39]	NOAA-GFDL, USA	50 km
CMIP6-HR	MPI-ESM1.2-XR[40]	MPI, Germany	40 km

The models include ENEA-REG, the CMIP6 and the CMIP6-HR.

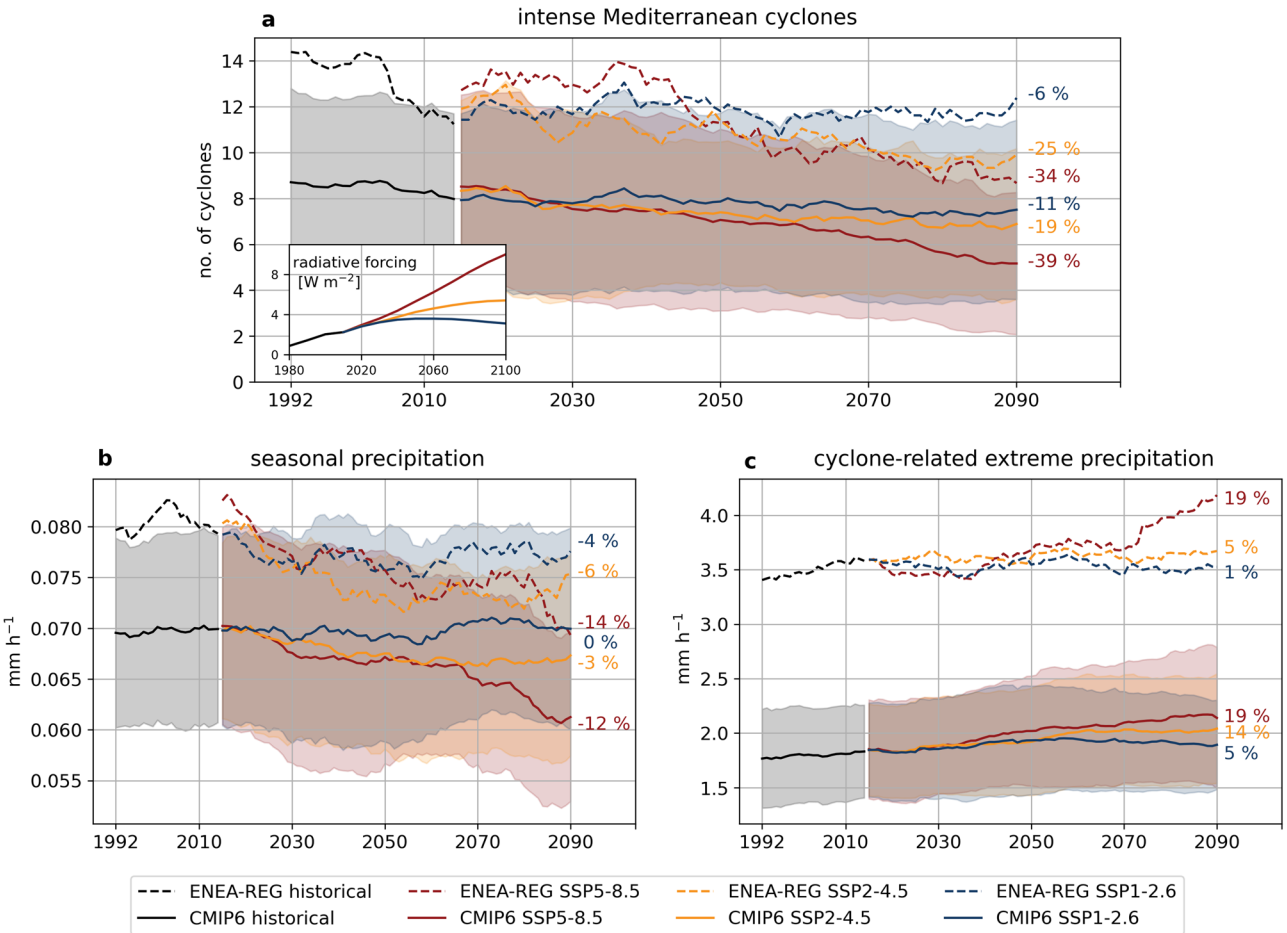

Fig. 1 | Temporal evolution of intense Mediterranean cyclones and associated extreme precipitation. Time series for **a** the number of intense Mediterranean cyclones, **b** seasonal Mediterranean precipitation (averaged over the Mediterranean domain outlined by dashed lines in Fig. S1) and **c** the extreme (99th percentile) precipitation associated with intense Mediterranean cyclones (averaged over the number of cyclones each year). All time series are smoothed using a 20-year moving average. Results are shown for the ONDJFM cold season in ENEA-REG (dashed lines) and the CMIP6 ensemble (solid lines), covering the historical period (black lines) and future scenarios SSP 5-8.5 (red), SSP2-4.5 (orange) and SSP1-2.6 (blue). The colour bands indicate the standard deviation for the CMIP6 ensemble. The percentages at the end of the time series show the changes of the end of the century compared to the historical mean. **a** includes an inset showing the evolution of anthropogenic radiative forcing under different SSP scenarios.

highlights the important role of Mediterranean cyclones on the extreme precipitation trends and reinforces the climate paradox for the Mediterranean basin[9]: if GHG emissions continue to rise, the region will experience lower seasonal precipitation, while even more extreme precipitation during intense cyclones. The combination of increased aridity[16] and amplified precipitation extremes is expected to heighten the risk of inland flooding from these storms, posing substantial challenges for the densely populated areas of the Mediterranean[17]. These findings motivate further investigation into the regional patterns of cyclone-related precipitation changes and their underlying physical drivers.

Figure 2 shows the regional patterns of the cyclone-related precipitation changes between the far-future (2071–2100) and the historical period (1985–2014). Higher levels of radiative forcing intensify the precipitation responses both in the regional and global models, with the former showing more pronounced changes. In all scenarios, a patchy response is observed: increased precipitation in northern, western and central Mediterranean regions, as well as along the Levantine coast, while decreasing in southern regions, especially over the Ionian and Aegean Seas and the Turkish coast. More specifically, while the frequency of intense storms is expected to decrease significantly under the high emission scenario (SSP5-8.5) in the central Mediterranean (Fig. S2a, b), reducing seasonal precipitation (Fig. S3a, b), the models project a marked increase in cyclone-related precipitation (Fig. 2a, b) over the Italian Peninsula and Balkan regions, where storms typically produce heavy rainfall (Fig. S4). This intensification is driven by the interaction between the cyclones and the complex orography of the basin, leading to intense precipitation over coastal areas, a feature captured only by the AORCM (ENEA-REG vs. CMIP6 in Figs. 2 and S4).

The projected increase in cyclone-related precipitation with climate change mainly results from moisture transport processes. In the ENEA-REG simulations, Mediterranean cyclones produce stronger 10 m wind speeds across most of the Sea under different emission scenarios (Fig. S5a, c, e). This, along with rising sea surface temperatures (SST, Fig. S6), fosters latent heat flux in the same areas (Fig. S7a, c, e), enhancing the vertical heat and moisture exchange from the ocean to the atmosphere during these storms. Additionally, at the mid-troposphere (500 hPa), increased moisture transport from the southwest (black arrows in Fig. 3a, c, e) provides further precipitable water to cyclones over the central Mediterranean, leading to higher relative humidity over the Italian Peninsula and the Balkans. This feature is captured only by the AORCM (shaded areas in Fig. 3) and helps explain the projected changes in cyclone-related precipitation under different SSP scenarios. The impact of climate change on both precipitation and related atmospheric processes during intense cyclones is stronger in both SSP5-8.5 (Figs. 2a, 3a, S5a) and SSP2-4.5 (Figs. 2c, 3c, S5c), while it remains more moderate under SSP1-2.6.

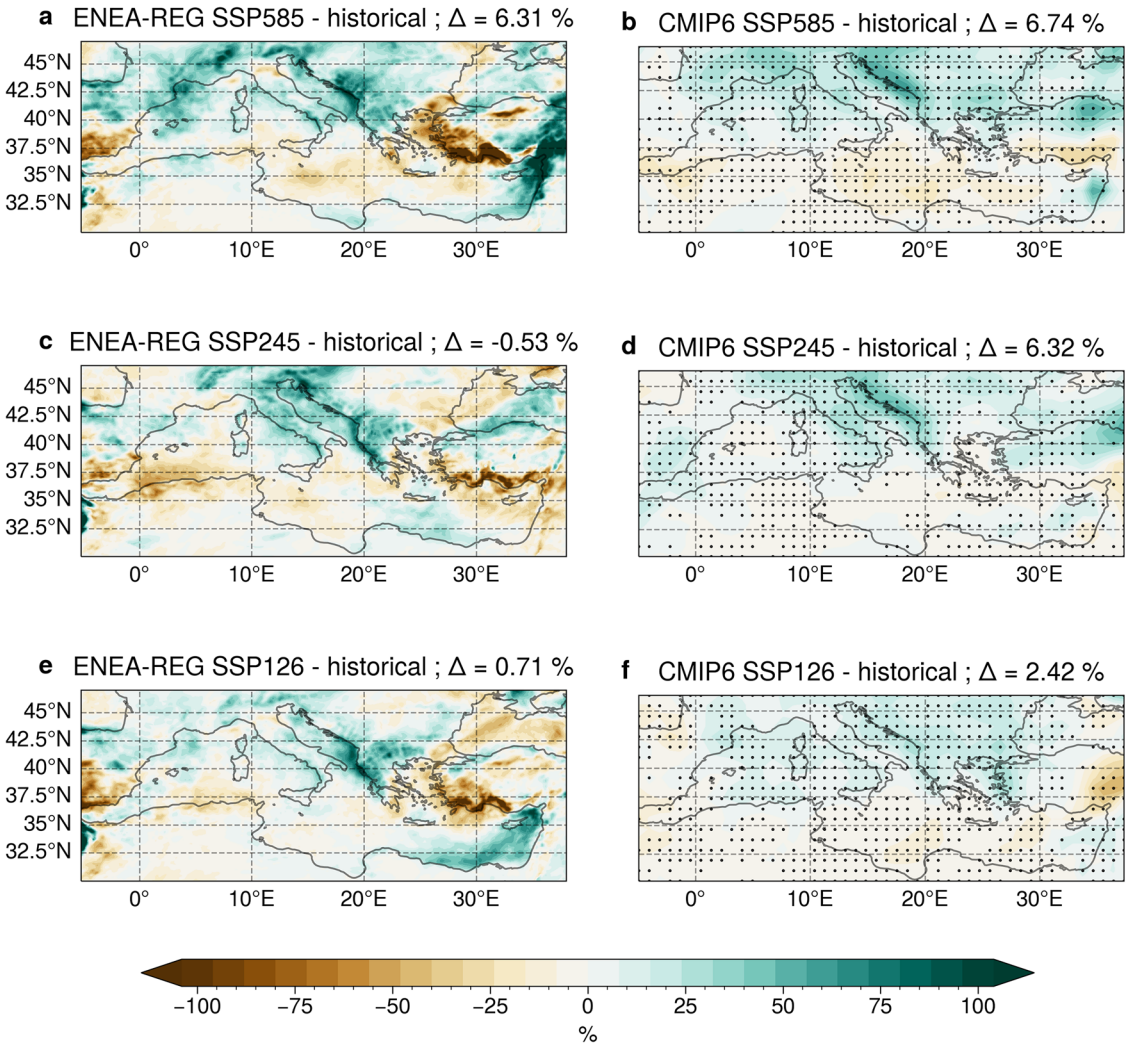

Fig. 2 | Cyclone-related precipitation changes. Maps of the differences in precipitation associated with intense Mediterranean cyclones between the far future (2071–2100) and the historical period (1985–2014), for SSP5-8.5, 2-4.5 and 1-2.6 scenarios. Results are shown for the ONDJFM cold season in ENEA-REG (**a**, **c**, **e**) and the CMIP6 ensemble (**b**, **d**, **f**). The differences are normalised by the historical mean value of cyclone-related precipitation. Black points on the CMIP6 maps indicate areas where at least four out of six models (i.e., more than 50%) agree on the sign of the difference. Δ values represent the domain average of the differences.

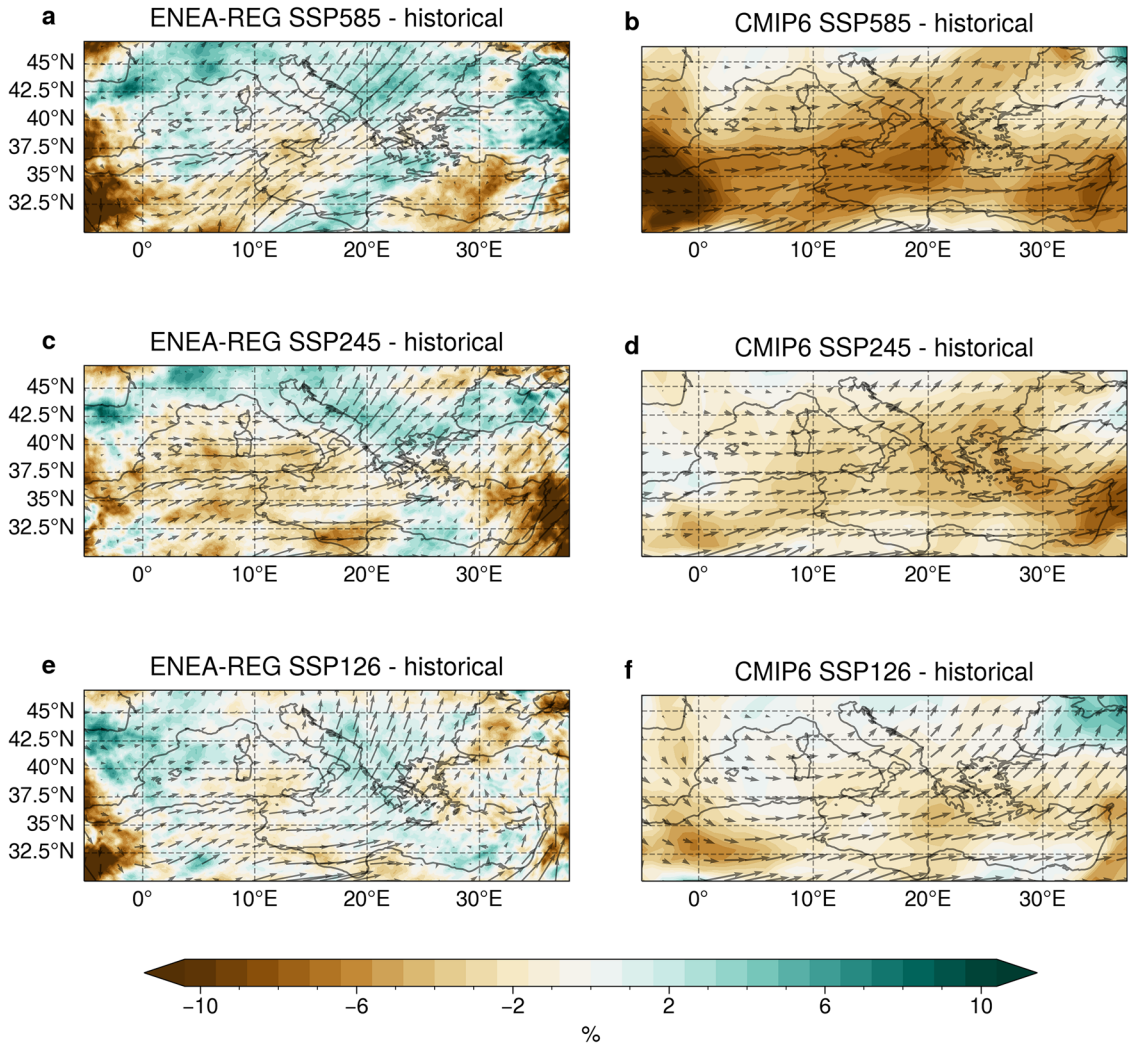

Fig. 3 | Cyclone-related mid-level moisture transport and relative humidity changes. Maps of the differences in moisture transport (black arrows) and relative humidity (shaded areas) at 500 hPa associated with intense Mediterranean cyclones between the far future (2071–2100) and the historical period (1985–2014), for SSP 5-8.5, 2-4.5 and 1-2.6 scenarios. Results are shown for the ONDJFM cold season in ENEA-REG (**a**, **c**, **e**) and the CMIP6 ensemble (**b**, **d**, **f**). The moisture transport is computed as the product of specific humidity and the horizontal wind speed vector, with arrows indicating the direction of the difference. In the CMIP6 maps, arrows are shown only for areas where at least four out of six models agree on the sign of the difference.

In contrast, under both SSP5-8.5 and SSP2-4.5, the southern Mediterranean is projected to experience pronounced drying (Fig. 2a, c) due to a decrease in cyclones frequency (Fig. S2a, c) and baroclinic forcing[9]. These changes lead to higher atmospheric stability and inhibition of convection, reducing 10 m wind speed and latent heat flux over the Ionian Sea (clearly visible only in ENEA-REG, Figs. S5a and S7a), which is the primary moisture source for storms in this region. However, ENEA-REG reveals a distinct response in the eastern Mediterranean: under the high-emission scenario, this region is projected to experience a significant increase in cyclone-related precipitation (Fig. 2a), primarily due to enhanced evaporation from the Sea (Fig. S7a) driven by both higher SSTs (Fig. S6a) and stronger surface winds (Fig. S5a).

These results highlight the ability of a high-resolution AORCM to coherently simulate the interconnected dynamic and thermodynamic processes during intense Mediterranean cyclones, providing new insights into how moisture is supplied during these events under different emission scenarios. This improvement stems from the model's finer representation of wind patterns and air-sea fluxes which influence cyclone-related precipitation[18,19]. Additionally, compared to the coarse CMIP6 models, AORCMs enhance the representation of Mediterranean Sea circulation[20] by resolving mass transport and energy flux exchanges through the Strait of Gibraltar[12]. Future changes in ocean circulation patterns (cyclonic and anticyclonic) modulate air-sea fluxes, affecting cyclone-related precipitation response[21]. While a multi-model ensemble helps identify robust precipitation signals under climate change (Fig. 2b, d, f), CMIP6 models struggle to capture the interaction between the Mediterranean Sea circulation and the local energy exchanges with the atmosphere, specifically the relation between changes in 10 m wind speed (Fig. S5) and latent heat flux (Fig. S7). In addition, they fail to accurately simulate the dynamics of moisture transport and the resulting changes in relative humidity (Fig. 3) over areas with complex orography.

These findings provide novel insights into the key role of cyclones on both the changing mean climate and extremes in the Mediterranean, offering valuable information for regional climate impact assessments and adaptation strategies. The analysis underscores the potential risk of more damaging inland flooding in a warming climate, particularly in southern Spain and France (including their islands), the Italian Peninsula, the Balkan region and the Levantine Coast, posing severe issues for such densely populated areas. Besides, our results highlight the importance of combing different models within coordinated frameworks to disentangle the influences of large-scale forcings and regional climate processes on the future

Mediterranean climate under varying radiative forcing levels. This approach is crucial for improving climate modelling and climate projections reliability.

Materials and methods

Models description

One high-resolution atmosphere-ocean coupled regional climate model (ENEA-REG[12]) and six CMIP6 global climate models (Table 1) are used in this study. Four different simulation periods are analysed, i.e., one historical (1982–2014) and three future scenarios (2015–2100): SSP5-8.5, SSP2-4.5 and SSP1-2.6.

ENEA-REG[12] simulates various components of the Earth system. The atmosphere is represented using the Weather Research and Forecasting model (WRF, version 4.2.2), the land processes are simulated using the Noah-MP scheme embedded within WRF, the Ocean circulation is reproduced using the Massachusetts Institute of Technology General Circulation Model (MITgcm, version Z67[22]), and freshwater fluxes are modelled using the Hydrological Discharge model (HD, version 1.0.2[23]). The model domain covers the Med-CORDEX region (Fig. S1) with a horizontal resolution of 12 km for the atmospheric component and approximately 10 km (1/12°) for the ocean component. In this study, ENEA-REG is initialised and forced by the MPI-ESM1-2-HR global model. The first two years of the historical simulation (1980–1982) are used as a spin-up period and thus the analysis is performed over the 1982–2100 timeframe.

The six CMIP6 global climate models were selected based on specific criteria. These criteria include a horizontal resolution finer than 100 km, comparable to that of the parent global model of ENEA-REG (MPI-ESM1-2.HR) and the availability of 6-hourly Sea Level Pressure (SLP) data required for the cyclone tracking algorithm. In addition, in the supplementary information, seven CMIP6-HR high-resolution global climate models are analysed for the historical experiment (Table 1), as the SSP scenarios are not available for these models. These high-resolution global models were chosen based on the availability of 6-h SLP data to meet the requirements of the tracking method.

Cyclone tracking algorithm

To identify Mediterranean cyclones, a cyclone tracking algorithm is applied to ENEA-REG, CMIP6 and CMIP6-HR simulations, as well as to ERA5 reanalysis, over the Med-CORDEX domain (Fig. S1). The tracking method is the same of Flaounas et al.[24] called "CycloTRACK", adapted from Flaounas et al.[25] and uses Mean Sea Level Pressure (MSLP), at 6 hourly intervals, to detect cyclone centres. Initially, a Gaussian filter with a 150 km kernel and a sigma value of 2 is applied to smooth the MSLP field. Cyclone centres are then identified as grid points with lower MSLP than their eight surrounding neighbours. Starting from the cyclone centre with deepest MSLP, the algorithm constructs potential tracks by connecting centres across consecutive time steps within a 250 km radius. From these candidates, the track with the smallest average MSLP difference is selected.

The MSLP fields of ENEA-REG, CMIP6 and CMIP6-HR are interpolated onto ERA5's regular grid (0.25°) before applying the cyclone tracking algorithm, to assure comparability between the models and the reanalysis[26] and to avoid tuning the algorithm parameters which are sensitive to the spatial resolution of the input SLP field and have been optimised based on ERA5 resolution. Cyclones over areas with altitudes above 800 m are filtered out, to exclude cyclone artefacts that form over mountains due to pressure field extrapolation to sea level[27]. Only cyclones with a minimum SLP below 1000 hPa and located within the area outlined by solid lines in Fig. S1[6] are classified as "intense Mediterranean cyclones" and included in this study. This allows to remove small cyclonic features that typically have limited influence on climate dynamics and extremes of the Mediterranean area[7].

The same methodology has been already applied in the hindcast (ERA5 driven) simulation of ENEA-REG, which highlighted how the model accurately represents the cyclone track statistics, i.e., intensity, lifetime and speed, as well as season cycle and spatial distribution[19].

Cyclone-related fields

To investigate the physical mechanism driving changes in cyclone-related precipitation, several fields have been analysed, including precipitation, 10 m wind speed, SST, latent heat flux, relative humidity at 500 hPa and mid-level moisture transport (specific humidity multiply be the wind speed vector at 500 hPa). The analysis is performed for both the regional and the global CMIP6 models at their original spatial resolutions. These fields are computed during the mature stage of each cyclone, defined as the timestep of the minimum SLP plus the two steps before and after it, totalling five time steps. The analysis is restricted to the area of influence of the cyclones, i.e., a circular disk with a 1000 km radius[6] around each SLP tracking points of the mature stage. To note that the models' output frequency is 6 h, thus the mature stage spans from 12 h before to 12 h after the time of the minimum SLP. For each grid point within the Mediterranean area (outlined by dashed lines in Fig. S1), the fields are averaged over all occurrences when a cyclone passes through that cell. These averaged fields are referred to as "cyclone-related fields". The precipitation differences are normalised by the mean historical value over the domain and expressed in percentage, Eq. (1):

$$\Delta = \frac{100\,(future - historical)}{historical\ mean}\ \%. \quad (1)$$

The extreme precipitation associated with intense Mediterranean cyclones (Fig. 1c) is computed for each cyclone as the 99th percentile of precipitation during its mature stage and within its area of influence (i.e., circular disk with a 1000 km radius). In the time series shown in Fig. 1c, each year's value represents the average extreme precipitation across all cyclones that occurred in that year.

Data availability

Enquiries about data availability should be directed to the authors.

Code availability

The main results of this work were obtained using Python. The codes are available upon request.

Received: 12 March 2025; Accepted: 9 June 2025;
Published online: 09 July 2025

References

1. Pozzer, G. Assessing hydrogeological vulnerability within northern apennines: an integrated spatial analysis in Emilia-Romagna Region (Italy). in *Climate Change Adaptation, Flood Risk, and Beyond.* 7–33 https://doi.org/10.1007/978-3-031-65463-3_2 (Springer Nature, 2024).
2. Piccolroaz, S. Devastating Spanish floods expose an urgent need for more flood-risk professionals. *Nature* **635**, 290–290 (2024).
3. Giorgi, F. Climate change hot-spots. *Geophys. Res. Lett.* **33**, L08707 (2006).
4. Tuel, A. & Eltahir, E. A. B. Why Is the Mediterranean a climate change hot spot? *J. Clim.* **33**, 5829–5843 (2020).
5. Flaounas, E. et al. Mediterranean cyclones: current knowledge and open questions on dynamics, prediction, climatology and impacts. *Weather Clim. Dyn.* **3**, 173–208 (2022).
6. Reale, M. et al. Future projections of Mediterranean cyclone characteristics using the Med-CORDEX ensemble of coupled regional climate system models. *Clim. Dyn.* **58**, 2501–2524 (2022).
7. Flaounas, E., Gray, S. L. & Teubler, F. A process-based anatomy of Mediterranean cyclones: from baroclinic lows to tropical-like systems. *Weather Clim. Dyn.* **2**, 255–279 (2021).
8. Allan, R. P. et al. Advances in understanding large-scale responses of the water cycle to climate change. *Ann. N. Y Acad. Sci.* **1472**, 49–75 (2020).
9. Zappa, G., Hawcroft, M. K., Shaffrey, L., Black, E. & Brayshaw, D. J. Extratropical cyclones and the projected decline of winter

Mediterranean precipitation in the CMIP5 models. *Clim. Dyn.* **45**, 1727–1738 (2015).
10. Insua-Costa, D., Senande-Rivera, M., Llasat, M. C. & Miguez-Macho, G. A global perspective on western Mediterranean precipitation extremes. *NPJ Clim. Atmos. Sci.* **5**, 9 (2022).
11. Xie, S.-P. et al. Towards predictive understanding of regional climate change. *Nat. Clim. Chang* **5**, 921–930 (2015).
12. Anav, A. et al. Dynamical downscaling of CMIP6 scenarios with ENEA-REG: an impact-oriented application for the Med-CORDEX region. *Clim. Dyn.* https://doi.org/10.1007/s00382-023-07064-3 (2024).
13. O'Neill, B. C. et al. The Scenario Model Intercomparison Project (ScenarioMIP) for CMIP6. *Geosci. Model Dev.* **9**, 3461–3482 (2016).
14. Ruti, P. M. et al. Med-CORDEX initiative for mediterranean climate studies. *Bull. Am. Meteorol. Soc.* **97**, 1187–1208 (2016).
15. Flaounas, E., Drobinski, P. & Bastin, S. Dynamical downscaling of IPSL-CM5 CMIP5 historical simulations over the Mediterranean: benefits on the representation of regional surface winds and cyclogenesis. *Clim. Dyn.* **40**, 2497–2513 (2013).
16. Seager, R. et al. Causes of increasing aridification of the Mediterranean region in response to rising greenhouse gases*. *J. Clim.* **27**, 4655–4676 (2014).
17. Cramer, W. et al. Climate change and interconnected risks to sustainable development in the Mediterranean. *Nat. Clim. Chang* **8**, 972–980 (2018).
18. Berthou, S. et al. Influence of submonthly air–sea coupling on heavy precipitation events in the Western Mediterranean basin. *Q. J. R. Meteorol. Soc.* **142**, 453–471 (2016).
19. Chericoni, M., Fosser, G., Flaounas, E., Sannino, G. & Anav, A. Extreme Mediterranean cyclones and associated variables in an atmosphere-only vs an ocean-coupled regional model. Preprint at https://doi.org/10.5194/egusphere-2024-2829 (2024).
20. Parras-Berrocal, I. M. et al. Response of the Mediterranean sea surface circulation at various global warming levels: a multi-model approach. *Geophys. Res. Lett.* **51**, e2024GL111695 (2024).
21. Jangir, B., Mishra, A. K. & Strobach, E. Effects of mesoscale eddies on the intensity of cyclones in the Mediterranean Sea. *J. Geophys. Res. Atmos.* **128**, e2023JD038607 (2023).
22. Marshall, J., Adcroft, A., Hill, C., Perelman, L. & Heisey, C. A finite-volume, incompressible Navier Stokes model for studies of the ocean on parallel computers. *J. Geophys. Res. Oceans* **102**, 5753–5766 (1997).
23. Hagemann, S. & Gates, L. D. Validation of the hydrological cycle of ECMWF and NCEP reanalyses using the MPI hydrological discharge model. *J. Geophys. Res. Atmos.* **106**, 1503–1510 (2001).
24. Flaounas, E. et al. A composite approach to produce reference datasets for extratropical cyclone tracks: application to Mediterranean cyclones. *Weather Clim. Dyn.* **4**, 639–661 (2023).
25. Flaounas, E., Kotroni, V., Lagouvardos, K. & Flaounas, I. CycloTRACK (v1.0) – tracking winter extratropical cyclones based on relative vorticity: sensitivity to data filtering and other relevant parameters. *Geosci. Model Dev.* **7**, 1841–1853 (2014).
26. Kouroutzoglou, J., Flocas, H. A., Keay, K., Simmonds, I. & Hatzaki, M. Climatological aspects of explosive cyclones in the Mediterranean. *Int. J. Climatol.* **31**, 1785–1802 (2011).
27. Neu, U. et al. IMILAST: a community effort to intercompare extratropical cyclone detection and tracking algorithms. *Bull. Am. Meteorol. Soc.* **94**, 529–547 (2013).
28. Wu, T. et al. The Beijing Climate Center Climate System Model (BCC-CSM): the main progress from CMIP5 to CMIP6. *Geosci. Model Dev.* **12**, 1573–1600 (2019).
29. Cherchi, A. et al. Global mean climate and main patterns of variability in the CMCC-CM2 Coupled Model. *J. Adv. Model Earth Syst.* **11**, 185–209 (2019).
30. Döscher, R. et al. The EC-Earth3 Earth system model for the Coupled Model Intercomparison Project 6. *Geosci. Model Dev.* **15**, 2973–3020 (2022).
31. Müller, W. A. et al. A Higher-resolution Version of the Max Planck Institute Earth System Model (MPI-ESM1.2-HR). *J. Adv. Model Earth Syst.* **10**, 1383–1413 (2018).
32. YUKIMOTO, S. et al. The meteorological research institute earth system model Version 2.0, MRI-ESM2.0: description and basic evaluation of the physical component. *J. Meteorol. Soc. Jpn. Ser. II* **97**, 931–965 (2019).
33. Seland, Ø. et al. Overview of the Norwegian Earth System Model (NorESM2) and key climate response of CMIP6 DECK, historical, and scenario simulations. *Geosci. Model Dev.* **13**, 6165–6200 (2020).
34. Wu, T. et al. BCC-CSM2-HR: a high-resolution version of the Beijing climate center climate system model. *Geosci. Model Dev.* **14**, 2977–3006 (2021).
35. Scoccimarro, E. et al. Extreme events representation in CMCC-CM2 standard and high-resolution general circulation models. *Geosci. Model Dev.* **15**, 1841–1854 (2022).
36. Saint-Martin, D. et al. Tracking changes in climate sensitivity in CNRM climate models. *J. Adv. Model Earth Syst.* **13**, e2020MS002190 (2021).
37. Haarsma, R. et al. HighResMIP versions of EC-Earth: EC-Earth3P and EC-Earth3P-HR – description, model computational performance and basic validation. *Geosci. Model Dev.* **13**, 3507–3527 (2020).
38. Roberts, C. D. et al. Climate model configurations of the ECMWF Integrated Forecasting System (ECMWF-IFS cycle 43r1) for HighResMIP. *Geosci. Model Dev.* **11**, 3681–3712 (2018).
39. Zhao, M. Simulations of atmospheric rivers, their variability, and response to global warming using GFDL's new high-resolution general circulation model. *J. Clim.* **33**, 10287–10303 (2020).
40. Gutjahr, O. et al. Max Planck Institute Earth System Model (MPI-ESM1.2) for the High-Resolution Model Intercomparison Project (HighResMIP). *Geosci. Model Dev.* **12**, 3241–3281 (2019).

Acknowledgements

This paper and related research have been conducted during and with the support of the Italian inter-university PhD course in Sustainable Development and Climate change (link:www.phd-sdc.it) and developed within the framework of the project "Dipartimento di Eccellenza 2023-2027", funded by the Italian Ministry of Education, University and Research at IUSS Pavia. This study is carried out within: ICSC Italian Research Center on High-Performance Computing, Big Data and Quantum Computing and received funding from the European Union Next-GenerationEU (National Recovery and Resilience Plan-NRRP, Mission 4, Component 2, Investment 1.4-D.D: 3138 16/12/2021, CN00000013); RETURN Extended Partnership and received funding from the European Union Next-GenerationEU (National Recovery and Resilience Plan NRRP, Mission 4, Component 2, Investment 1.3-D.D. 1243 2/8/2022, PE0000005); CoCliCo (Coastal Climate Core Service) research project which received funding from the European Union's Horizon 2020 Research and Innovation Programme under Grant agreement No. 101003598; CAREHeat (deteCtion and threAts of maRinE Heat waves) project, funded by the European Space Agency (ESA, grant agreement no. 4000137121/21/I-DT). We acknowledge the World Climate Research Programme, which, through its Working Group on Coupled Modelling, coordinated and promoted CMIP6. Within this we thank the CMIP6 endorsement of the High-Resolution Model Intercomparison Project (HighResMIP) and Martin Schupfner for providing additional data from the MPI-ESM. The computing resources and the related technical support used for this work have been provided by CRESCO/ENEA-GRID High Performance Computing infrastructure and its staff. This article is based upon work from COST Action CA19109 "MedCyclones", supported by COST - European Cooperation in Science and Technology (http://www.cost.eu).

Author contributions

M.C., G.F., and A.A. conceived the idea of the manuscript. M.C. performed the analysis and wrote the manuscript with inputs from all the authors. A.A.

developed the ENEA-REG model and performed the simulations. E.F. developed the cyclone tracking algorithm.

Competing interests
The authors declare no competing interests.

Additional information
Supplementary information The online version contains supplementary material available at https://doi.org/10.1038/s41612-025-01121-w.

Correspondence and requests for materials should be addressed to Marco Chericoni.